



# Artificial neural network-based maximum power point tracking controller for real-time hybrid renewable energy system

Mohammad Junaid Khan<sup>1</sup> · Lini Mathew<sup>2</sup>

Accepted: 2 February 2021 / Published online: 25 February 2021

© The Author(s), under exclusive licence to Springer-Verlag GmbH, DE part of Springer Nature 2021

## Abstract

Development of various maximum power point tracking (MPPT) control techniques for proposed systems such as solar photo-voltaic (PV), wind turbine (WT), fuel cell (FC) and hybrid renewable energy system (HRES). HRES is the combination of PV, WT and FC which is connected parallelly by DC link. It is implemented in real-time using OPAL-RT system. In this research article, the MPPT algorithms viz. Perturb and Observe (P&O), Fuzzy Logic (FL), Artificial Neural Network and Adaptive Neuro-Fuzzy Inference System (ANFIS) have been analyzed and compared. Results have been carried out to record tracking performance of MPPT controllers by introducing changes in the radiation, wind speed hydrogen fuel rate. It has been observed that the proposed HRES using ANFIS-based MPPT controller provides better response as compared to other specified MPPT controllers.

**Keywords** ANFIS · ANN · FC · FL controller · Hardware in the loop (HIL) · HRES · MPPT algorithms · OPAL-RT simulator · P&O · Power converters · PV and WT

## 1 Introduction

In recent years, the rising ecological issues such as greenhouse gas emission and energy cost have motivated novel research into alternative approaches of production of electrical power. An enormous deal of new research is going on to search out for non-polluting renewable energy sources and explore the precision of renewable energy frameworks to enhance the efficiency and reduce the cost of power in per peak watt (Khan et al. 2017; Yadav et al. 2018; Khan 2020; Kewat et al. 2018). A dynamic prototype of an HRES including a wind-driven self-excited induction generator, PV framework and the power preparing circuit has been developed (Valenciaga and Puleston 2005). A modest and cost-effective MPPT algorithm has been presented for the solar PV and WT without evaluating the

ecological situations (Giraud and Salameh 2001). Maoum et al. have presented experimental and theoretical examine for the appraisal of fast and reliable MPPT control methods, for example, voltage- and current-based MPPT techniques for PV systems (Masoum et al. 2002).

Kamal et al. proposed control technique develops FL-based MPPT controller for providing the maximum power coefficient for a static pitch and sudden changes of load (Kamal et al. (2010)). Rowe et al. established a one-dimensional non-isothermal prototypical of a proton exchange membrane FC (PEM-FC) and analyzed the impact about different outline and working states on the cell performance, thermal response, and water controlling to realize the underlying mechanism (Rowe and Li 2001).

A non-recurrent radial-basis-function ANN has been employed to build meta models to signify the steady-state associations among the stack power, the compressor voltage, the stack current, and the oxygen movement (Hasikos et al. 2009).

Real-time simulation-based comparative analysis of FL, ANN, ANFIS techniques using MATLAB<sup>TM</sup>/ dSPACE<sup>TM</sup> platform for PV system shows the better performance of ANFIS-based MPPT technique as compared to other control methods (Karanjkar et al. 2014a). ANFIS and ANN

✉ Mohammad Junaid Khan  
junaid.elect@nittrchd.ac.in

<sup>1</sup> Department of Electrical and Electronics Engineering, Mewat Engineering College, Nuh, Haryana, India

<sup>2</sup> Department of Electrical Engineering, National Institute of Technical Teachers Training and Research, Chandigarh 160019, India

algorithms are used to predict SOFC performance by supplying power and heat to a residence. The result shows the significant reduction in favor of computational time without affecting the accuracy of SOFC model (Entchev and Yang 2007).

The integration of PV, WT, and diesel generator (DG), i.e., hybrid system has been proposed using an ANFIS-based MPPT technique and the simulation results yield the power generation and consumption are encouraging in terms of their stability (Sharma and Soni 2016). After a comparative analysis of various MPPT techniques for Wind-PV hybrid system, the results show the effectiveness of ANFIS-based MPPT technique in terms of voltage level and minimization of fluctuation about maximum power point (MPP) (Ali 2014).

A voltage MPP technique has been presented in which the reference voltage is dynamically tracked online escaping the necessity to disrupt the main circuit as completed in the conservative constant voltage technique (Leedy et al. 2012). A comparative analysis of two most common MPPT techniques specifically modified P&O-based MPPT- and INC-based MPPT technique has been considered (Shankar et al. 2013). Experimental analysis of design and development of an independent WT, solar PV, diesel, and batteries power framework has been presented (Tudorache et al. 2012). Hybrid optimization model for electric renewable (HOMER) is a software which establishes on the RE achievable for the installation site and taking into justification levied daily load profiles. The control algorithms and design approach for 1–5 kW stand-alone hybrid solar PV and WT system have been introduced (Meiqin et al. 2008). The experimental and simulation results illustrate that the proposed control and design approach, WT and PV module operate at MPP and battery bank may remain in the drift alleging state, improving the cycle-rate and extend the life in favor of the batteries. A control method has been suggested for a hybrid WT–PV–battery system by the concern of battery outcome with the linear expectation of WT and solar PV framework using FL controller-based MPPT technique used for the battery during charging and discharging (Mousavi et al. 2009).

In this paper, the various MPPT controllers viz. P&O, FL, ANN, and ANFIS have been implemented on real-time using OP4510 for PV with boost converter, WT with buck converter, FC with boost converter and HRES with dc–dc converters. Comparative analyses of these controllers for rapid change in solar radiation and wind speed have been presented. Real-time implementation of proposed models with various MPPT controllers have been done by OP4510 simulator which is family of OPAL-RT technology. Voltage and current sensors necessary for MPPT algorithms and maximum power calculations have been designed and interfaced using connectors and PV emulator, WT

emulator, FC and HRES input–output (I/O) board. This paper has been organized in the following sequence:

Sections 2 and 3 details about the hardware involved in the development of laboratory prototype and experimental procedure. Model development for real-time implementation of MPPT (P&O, FL, ANN, and ANFIS)-based controllers have been discussed in Sect. 4. Section 5 reports about the results of real-time simulations and comparative analysis of the above mentioned different MPPT controllers, Sect. 6 comparative analysis of various MPPT controllers for different systems in OPAL-RT, followed by conclusion in Sect. 7.

## 2 Development of prototype of PV, WT, FC, and HS

Laboratory prototype of the PV, WT, FC, and HS used to perform all the experimental studies includes: (1) PV emulator, (2) WT emulator, (3) FC system, (4) HS, (5) dc–dc converters, (6) resistive load, (7) OPAL-RT simulator (8) sensor circuits for measurement of voltage and current and (9) personal computer with MATLAB/SIMULINK and RT-LAB software. The MPPT controllers for various MPPT techniques have been designed on MATLAB/SIMULINK platform and have been burnt on OPAL-RT simulator. Analysis of the real-time operation of MPPT controllers has been carried out using RT-Lab software. Details of these hardware components and step-by-step experimentation procedure have been discussed in the following sub-sections.

### 2.1 Hardware components of the prototype

Laboratory prototype consists of PV emulator with a boost converter, WT emulator with buck converter and FC system with a boost converter. These converters are controlled by PWM using different MPPT controllers in OPAL-RT simulator. Voltage and current signals are sensed by using voltage and current sensors, and these signals are then provided to the input of OPAL-RT simulator. Block diagram of a laboratory prototype setup as shown in Fig. 1.

In Fig. 1, 1 & 2, 3 & 4, 5 & 6, 7 & 8, 9 & 10, and 11 & 12 are the voltage divider resistors. V1, V2, V3, V4, V5, and V6 are voltage sensors. C1, C2, C3, C4, C5, and C6 are current sensors. 13 is the dc-link capacitor. 14 is the resistive load. V1, V3, and V5 are the analog voltage signals and C1, C3, and C5 are the analog current signals as of input side of dc–dc power converters which are sensed by voltage and current sensors, respectively. Similarly, for the output side of dc–dc power converters, V2, V4, and V6 are the analog voltage signals and C2, C4, and C6 are the

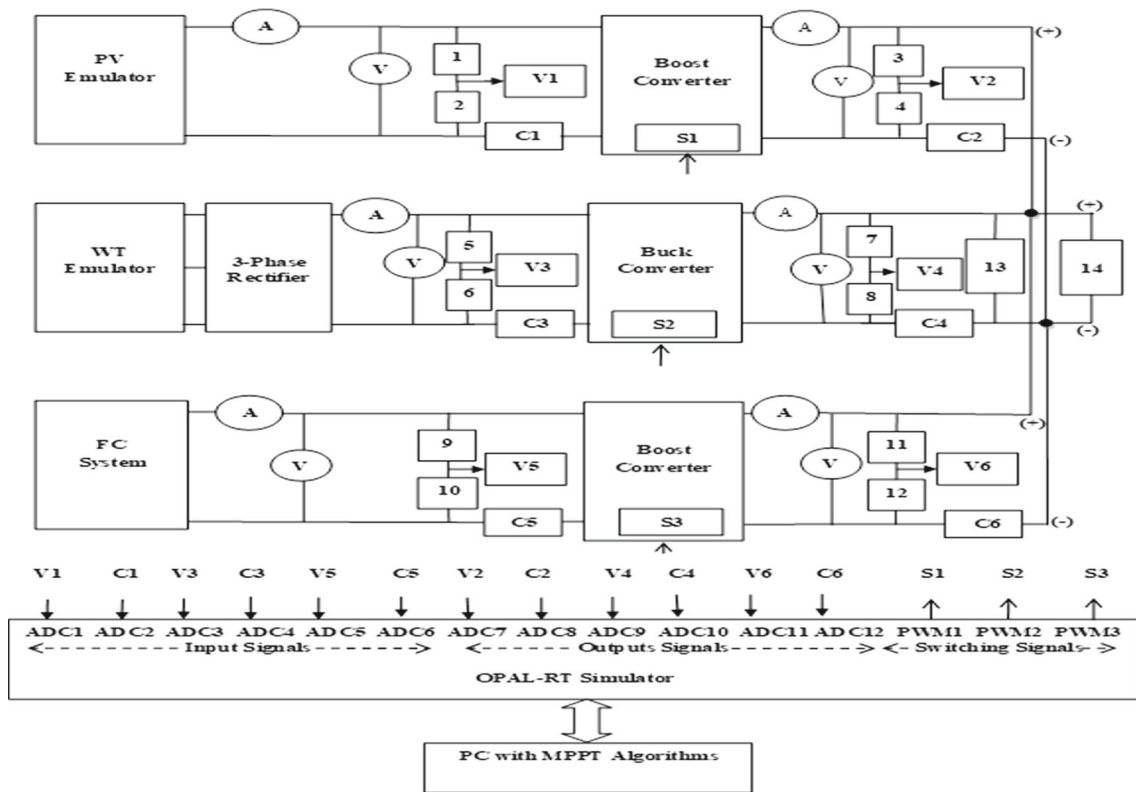


Fig. 1 Block diagram of laboratory prototype setup

analog current signals which are sensed by voltage and current sensors, respectively.

PWM1, PWM2, and PWM3 are the pulse width modulation which generate switching signals (S1, S2, and S3) or control signals by OPAL-RT simulator for dc-dc converters.

### 2.1.1 Solar photo-voltaic emulator

The PV Emulator uses an internal algorithm to adjust  $V_{OC}$  (Open circuit voltage) and  $I_{SC}$  (short-circuit current) so as to match the solar panel selected by the user based on ambient temperatures, solar radiation levels, etc. The power output by solar panels depends on a lot of parameters. These parameters are dynamic and interdependent, making it a complex process to predict the response of the PV system. PV emulator takes into account the weather conditions at the time of year specified, the position of the sun at the hour specified, the location of the panel, the positioning of the panel and technology, and manufacturer of the panel to estimate the response the solar panel. The emulator then makes sure the response matches to that of the actual panel under all the load conditions within range. The user is presented with a complete set of information with tables and plots on user application. The emulator is capable of storing up to twenty-five  $I-V$  curves into its

memory, with a programmed time interval range of one hour. It can emulate the  $I-V$  curve for the complete day for PV inverter testing or dynamic  $I-V$  curve transient testing. Solar PV emulator is shown in Fig. 2 and its specifications are given in Table 1.

### 2.1.2 Wind emulator

Of the available alternatives, wind energy has emerged as one of the most established technologies. However, the output of Wind Energy Conversion System (WECS) is



Fig. 2 Solar PV emulator

**Table 1** Specifications of PV emulator

Input	Supply voltage	230 V AC, 50 Hz
	Short-circuit current ( $I_{sc}$ ) per Channel	0–8 A
	Open circuit voltage ( $V_{oc}$ ) per channel	0–50 V DC
	maximum output power per channel	400 W
Output	Maximum channels in series/parallel	4
	maximum absolute voltage at output	200 V DC
	Voltage slew rate range	0.01–2 V/ms
	Current slew rate range	0.01–1A/ms or Inf
	Mode of operation	Fix, table, simulator and programming modes
	Connector at output	Banana type
	Operating environment	Indoor use

dependent on wind flow which by nature is erratic and unpredictable. So far, the development of the control scheme and ensuring a reliable WECS has been a major area of focus. However, the efficacy of the control scheme can be assured by several experiments with an actual WT. Dependency on actual WT is ultimately dependency on environmental conditions. Such dependencies may cause indefinite delays. Moreover, several worst cases for which system needs to be tested may never occur and thus performance and reliability of controllers for those cases are always questionable. Another way is to set up a WT in a laboratory. It is difficult to set up a WT in the laboratory because of challenges like space and controlled environment, for example, wind tunnel. A solution of these problems can be found in a WT Emulator.

WT emulator mimics the behavior of actual WT under controlled manner. Essentially, it simulates the same operating pattern at the hardware level in real time similar to what an actual WT does at given operating parameters of wind speed and pitch angle. Term emulation is coined for simulation practices which involve hardware platform. In simple words, emulation is hardware level simulation. It provides a fast-configurable testing platform. Usually, these are performed in real time. The emulator is similar to Hardware-In-Loop simulation concepts.

WT emulator can find applications in numerous fields. It provides a flexible testing platform for the study of the dynamic and steady-state behavior of WT. Beginners can learn about power-wind speed, torque-turbine speed and power-turbine speed characteristics of a WT and can do comparative studies about how changes in parameters of WT affect the behavior. For other applications, this emulator can be coupled to the generator (Induction, PMSG, DFIG) followed by power electronics in place of actual WT. So, researchers would not have to rely on environmental conditions which are appropriate for driving the WT at some desired operating point. Since the operating point of wind emulator can be controlled, the researcher can simulate all possible scenarios of operation of WT and

accordingly can modify the power electronics and control algorithms. Consequently, it will improve product quality and reliability. WT emulator is illustrated in Fig. 3 and its specifications are given in Table 2.

### 2.1.3 FC system

A Proton Exchange Membrane fuel cell (PEMFC) is a device that converts hydrogen and oxygen into electricity and water. It uses a water-based, acidic polymer membrane as its electrolyte, with platinum-based electrodes. FC operate at relatively low temperatures (below 100 °C) and can adapt electrical output to meet dynamic power necessities. Due to the relatively low temperatures and the use of precious metal-based electrodes, these cells must operate on pure hydrogen. FC system is presently leading technology for light-duty vehicles and materials handling vehicles, and to a lesser extent for stationary and other applications.

Figure 4 shows the Fuel cell system and its specifications are given in Table 3.

**Fig. 3** Wind emulator

**Table 2** Specifications of wind emulator

DC motor	Out power	3.5 kW (5HP)
	Nominal field voltage	220 V DC
	Nominal armature	220 V DC
	The speed at rated voltages	1500
DC drive	Input voltage	Single phase AC
	DC link capacitor	3300 $\mu$ F, 450 V DC
	Control	Fix field
	Rating	15 A, 250 V DC
Gear box	Switching frequency	60 kHz
	Gear ratio	2:1
	Type	Squirrel cage type
induction generator	Output power	1.2 kW
	The line to line voltage	415 V AC
	No. of poles	8
	Input voltage	24 V DC
Techo-generator	Speed encoding	10 V DC for 1500 rpm
	Connection	Delta
AC excitation capacitor	Capacitance	50 $\mu$ F AC
	Technology	FPGA
Control card	ADC inputs	Available
	PWM ports	Available
	Rating	10 A, 400 V
Bridge rectifier	Capacitor	3300 $\mu$ F, 450 V

**Fig. 4** Proton exchange membrane fuel cell system

### 3 Proposed HS using OPAL-RT simulator

The investigator has developed the HS consisting of PV emulator with a boost converter, WT emulator with buck converter, FC system with a boost converter, Opal-RT simulator, computer system and dc link as per the block diagram of Fig. 1. This is the setup in the Power Electronics Laboratory of National Institute of Technical Teachers Training and Research Chandigarh. The advantage of the HS is that it can achieve the maximum power continuously during any one system is in running condition. The hardware setup of the proposed HS is shown in Fig. 5.

**Table 3** Specifications of PEMFC

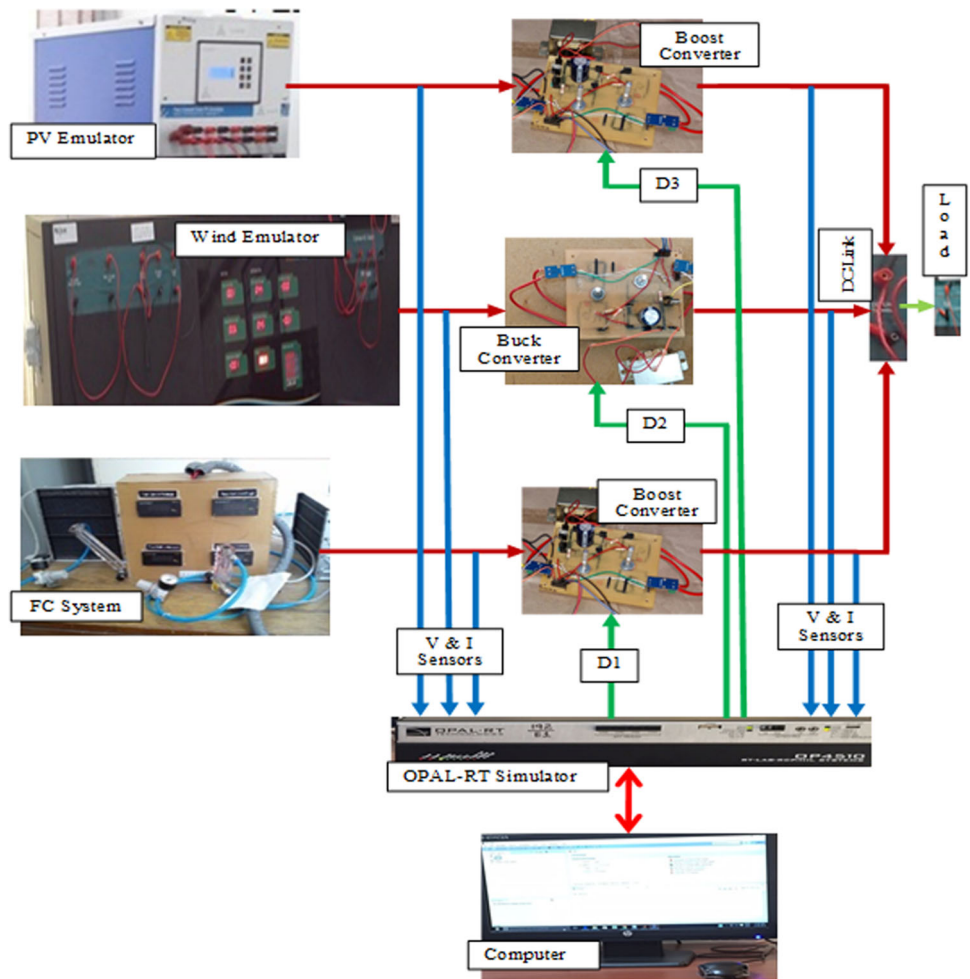
No. of cells	48
Nominal rated power	1000 W
Performance	35A, 28.8 V
Maximum stake temperature	65 °C
Hydrogen pressure	0.55–0.55 bar
Hydrogen purity	$\geq 99.995\%$
Flow rate at maximum output	13 L/minute
Start-up time	$\leq 30$ s at Ambient Tem
Efficiency of stake	40%
Low voltage shut down	24 V
Over current shunt down	42 A
Over temperature shut down	65 °C
External power supply	8 A, 13 ( $\pm$ V)

#### 3.1 DC–DC converter

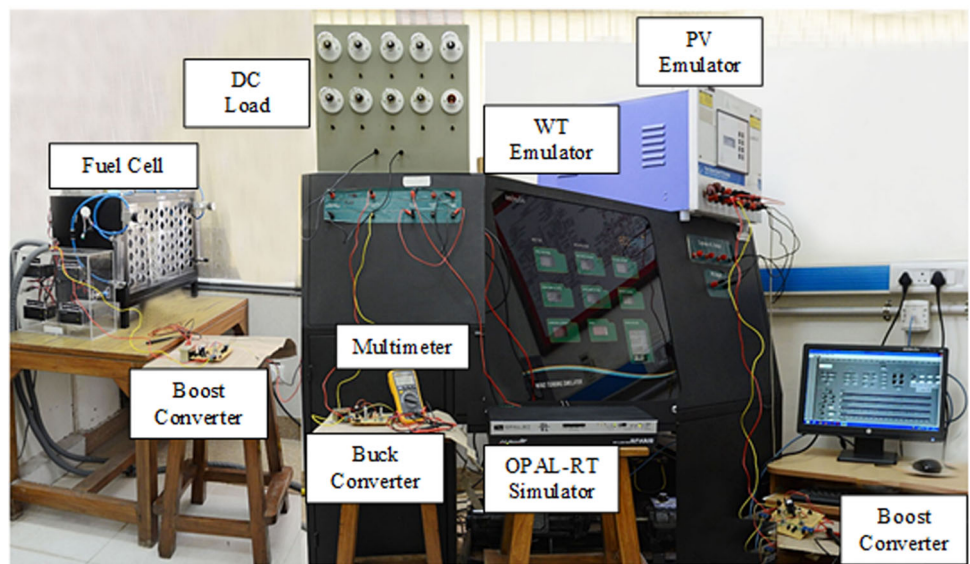
Design specifications of a boost converter for PV and FC model and buck converter for the WT model are given in Tables 4 and 5.

The dc–dc converters have been designed using IRF840 MOSFET and IN5408 diode. This is used for real-time implementation system. Photograph snaps of the buck, and boost converters are shown in Fig. 6.

**Fig. 5** Laboratory prototype of proposed HS (a) connection diagram (b) Complete hardware setup



(a)



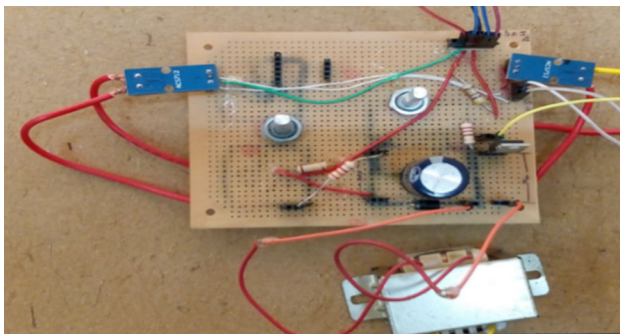
(b)

**Table 4** Buck Converter Parameters

Parameter	Value
Inductor (L)	3 mH
Output Capacitor ( $C_0$ )	470 $\mu$ F
Switching frequency ( $f_s$ )	10 kHz
Input Voltage (V)	300 V
Duty ratio (D)	Variable
Load resistance	100 $\Omega$

**Table 5** Boost converter parameters

Parameter	Value
Inductor (L)	3 mH
Output capacitor ( $C_0$ )	470 $\mu$ F
Switching frequency ( $f_s$ )	100 kHz
Input voltage (V)	88 V
Duty ratio (D)	Variable
Load resistance	100 $\Omega$



(a)



(b)

**Fig. 6** Photograph snaps of DC–DC converter (a) buck converter and (b) boost converter

### 3.2 Sensor design

For the different types of MPPT techniques, current and voltage are required to be interfaced by computer system via OPAL-RT controlling board. Current and voltage sensors have been designed and calibrated for implementation of different MPPT algorithms. The voltage sensor is designed using voltage divider resistive network. This is illustrated in Fig. 7.

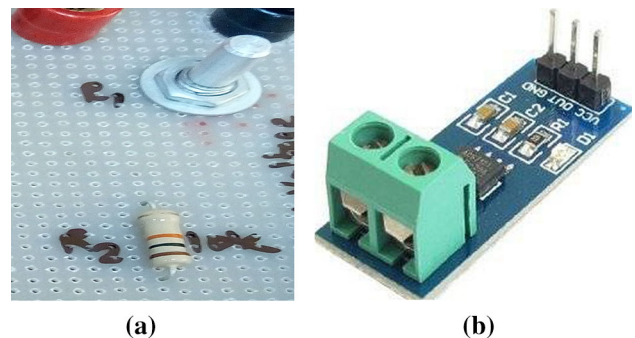
The output voltage is sufficiently reduced by adjusting the value of the variable resistor to 470 K and input voltage is sufficiently reduced by adjusting the value of the variable resistor to 2.5 K. As per the specifications of OPAL-RT system, it accepts analog input in the range of  $\pm 16$  V. Current measurement has been done using current sensor ACS712 that will produce an output voltage proportional to the current flowing through it.

### 3.3 OPAL-RT simulator

OPAL-RT is the world leader in the development of PC/FPGA-based Real-Time Digital Simulator, Hardware-In-Loop (HIL) testing equipment and Rapid Control Prototyping (RCP) systems to design, test and optimize control and protection systems used in power electronics, power grids, motor drives, automotive industry, trains, aircrafts and various industries, as well as R&D centers and universities.

OPAL-RT introduces a whole range of RCP solutions in order to iterate and test, quickly develop, cut back lying on development risks, cost, time, and control strategies. The advantage of OPAL-RT over another simulator is the HIL simulation which offers complexity and time in order to market.

It is affordable and compact real-time digital simulators with the power grid and also provides a new level connectivity, versatility and expandability to the platform. It has eMEGAsim RT-LAB software (Pak et al. 2006) and the specification of OPAL-RT simulator (Khan and Mathew 2018).



(a)

(b)

**Fig. 7** a Voltage sensor. b Current sensor

### 3.4 Experimentation procedure

SIMULINK™ is a software program in MATLAB™ with which one can perform model-based control system design. The I/O ports of OP4510 are accessible from the Simulink library browser. The control system designed in the SIMULINK™ for MPPT, using SIMULINK™ and OPAL-RT simulator, can be downloaded into the OP4510 board to run in real-time using ‘build’ option in the Simulink configuration setting.

The procedure to build SIMULINK™ model on OP4510 controller board is as follows: open SIMULINK™ model, click on configuration parameters in Simulink menu. Select ‘solver’ enter ‘inf’ in the text box for simulation stop time. Select ‘fixed step’ in solver type enter ‘0.001’ (or as appropriate for real-time simulation of the MPPT technique) in the text box for ‘fixed step size.’ Uncheck ‘block reduction’ option in the ‘optimization’ window. Then, select ‘code generation’ and browse and select ‘rti7104.tlc’ in the system target file text box. The model can be sent to OP4510 using ‘build’ option in the ‘code generation’ window shown in Fig. 8.

The fixed step size is similar to the discrete-step, which has been used by OP4510. This means that in every step-time the whole program will be executed, decision making will be done inside OP4510 and I/O data will be exchanged. During the build process of the SIMULINK model:

- (1) Compilation of C-code is done which will be used to implement the Simulink model in the OP4510 and
- (2) A supported file will be created which will be used by meta controller to access the variables of the SIMULINK™ model.

The RT-LAB window is RT-LAB’s graphical user interface. It enables the client to experience the whole

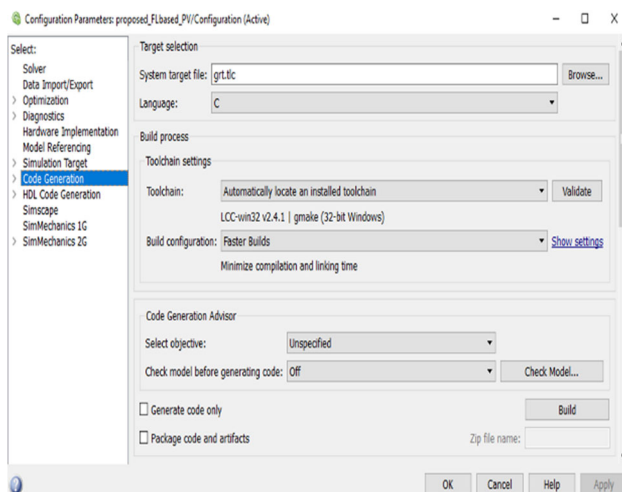


Fig. 8 ‘Configuration parameters’ settings for real-time interface

execution process and to get to the different capacities and operations offered by RT-LAB as appeared in Fig. 9. It has connections to different utilities and propelled highlights. The Meta Controller application must keep running before beginning the RT-LAB window.

### 4 Real-time implementation of MPPT controllers

In the current work, different MPPT control methods have been programmed with MATLAB™ and implemented using OPAL-RT OP4510 simulator, PV emulator with a boost converter, WT emulator with buck converter, FC system with boost converter, and proposed hybrid renewable energy system with different MPPT controllers. Analog signals are sensed by current and voltage sensors which are then fed to the OPAL-RT simulator for processing. The different MPPT controllers designed and simulated employing the PC and OP4510, generated the duty ratio  $D$ . The value of  $D$  is then fed to the buck and boost converters, and the output voltage and current are measured.

The investigator carried out the experimentation separately one by one as follows:

- (1) PV system with boost converter incorporated with
  - (a) P&O MPPT controller
  - (b) FL-based MPPT controller
  - (c) ANN-based MPPT controller
  - (d) ANFIS-based MPPT controller
- (2) WT system with buck converter incorporated with

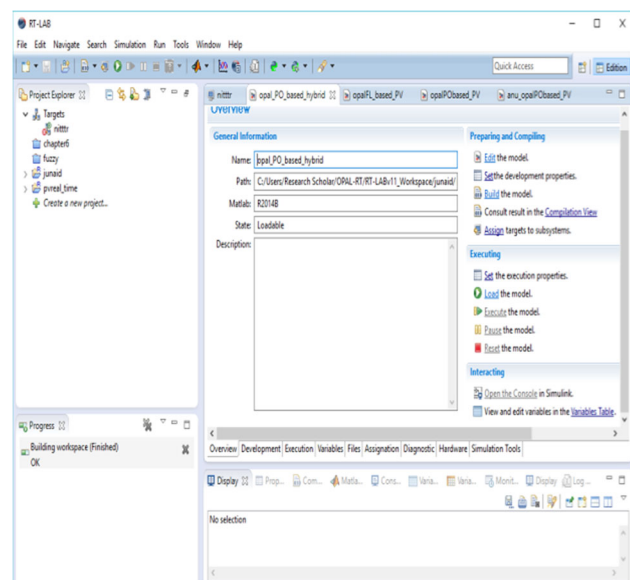


Fig. 9 View of RT-Lab window



- (a) P&O MPPT controller
  - (b) FL-based MPPT controller
  - (c) ANN-based MPPT controller
  - (d) ANFIS-based MPPT controller
- (3) FC system with boost converter incorporated with
- (a) P&O MPPT controller
  - (b) FL-based MPPT controller
  - (c) ANN-based MPPT controller
  - (d) ANFIS-based MPPT controller
- (4) HS (as shown in Fig. 5) incorporated with
- (a) P&O MPPT controller
  - (b) FL-based MPPT controller
  - (c) ANN-based MPPT controller
  - (d) ANFIS-based MPPT controller

The results and comparative analysis also have been investigated.

### 4.1 Model of P&O-based MPPT controller

In P&O, current and voltage of the framework are measured and resultant power  $[P_1(k)]$  is calculated.

After that including small perturbation of voltage ( $\Delta V$ ) or perturbation of duty ratio ( $\Delta D$ ) of the dc–dc converter in one direction, corresponding power  $[P_2(k)]$  is calculated. Power  $[P_2(k)]$  is next compared with power  $[P_1(k)]$ . If  $[P_2(k)]$  is greater than  $[P_1(k)]$ , then the perturbation is in the accurate direction, else, perturbation direction to be reversed. By this technique, the maximum power point (MPP) is reached. Then, the framework will oscillation around the MPP under steady state. These fluctuations are responsible for the energy loss and therefore, cause a reduction in efficiency. Flowchart of P&O control method is shown in Fig. 10 (Karanjkar et al. 2014b, c).

Figure 11 shows the subsystem of P&O MPPT Controller for PV, WT, FC, and HS, respectively.

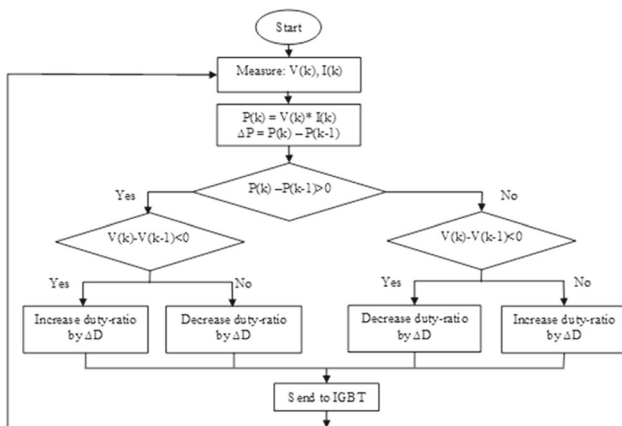


Fig. 10 Flowchart of P&O MPPT control method

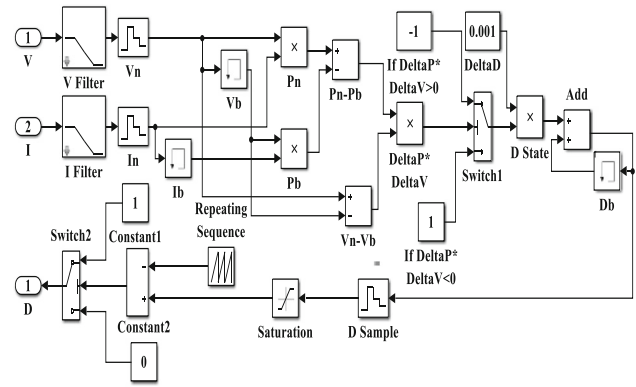


Fig. 11 Subsystem of P&O MPPT controller

MATLAB™/ SIMULATION™ platform is used for computing the MPP based on P&O technique. This technique receives voltage and current data for computing duty ratio ( $D$ ).

The SIMULINK/OPAT-RT-based model of P&O-based MPPT controller is shown in Fig. 12. The initial value of the duty ratio is 0.8. ADC channel one has been used to log PV current while channel five has been used for PV voltage. PWM channel number two of OP4510 has been used to provide a pulse width modulated signal of 10 kHz frequency to the MOSFET driver circuit of the dc–dc converter.

The MPPT parameter block is used to set nominal values of the duty ratio that is 0.8, the minimum and maximum limits of the duty ratio (0.1 and 0.8) and the perturbation in duty ratio  $\Delta D$ . This procedure is followed in PV, WT, FC and HS. P&O-based MPPT controller has been analyzed for  $\Delta D = 0.001$  in this study. Using this method, the maximum value of the power ( $P_{max}$ ) has been determined from the overall developed system.

### 4.2 Model of FL-based MPPT controller

MPPT methods based on artificial intelligence techniques have become more prevalent as compared to the conventional methods in recent years, because of very good and fast response, without overshoot and fewer fluctuations

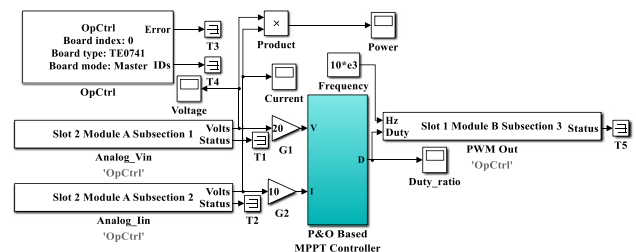


Fig. 12 Model of P&O-based MPPT controller in SIMULINK/ OPAL-RT

under rapid variations in temperature, radiation, and wind speed. The FL-based method does not require the exact model of a PV system for its design (Karanjkar et al. 2014b, c). In most of the literature, FL-based MPPT has been proposed with two inputs and one output. The two input variables are taken as: (1) error  $E(k)$  and (2) change in error  $\Delta E(k)$ . They are given by (Algazar et al. 2012):

The fuzzy inference can be carried out by one of the different available methods. FL controller Mamdani's method has mostly been used, and center of gravity defuzzification method is used to compute the output (change in duty ratio,  $\Delta D(k)$ ). The scheme of such an MPPT technique is shown in Fig. 13.

In FL controller design, one should identify the main control variables and determine the sets that describe the values of each linguistic variable and their range. The input variables are error  $E(k)$  and the change in error  $\Delta E(k)$ . These input signals are calculated and converted into linguistic variables. The output of the FL is the change in duty cycle  $\Delta D(k)$ . FL-based MPPT subsystem has been designed by two input variables viz. error and change of error and one output variable viz. change in duty ratio ( $\Delta D$ ) is shown in Fig. 14 and Fig. 15.

In the FL-based MPPT, the variables such as error and change in error are fuzzyfied into membership value by triangular membership function. The interval of  $(-5, 5)$  is used for input variables  $E(k)$  and  $\Delta E(k)$  and for output variable  $\Delta D$   $(-0.2, 0.2)$  for PV system (Hasikos et al. 2009).

Seven fuzzy sets are considered for membership functions, these variables are expressed in terms of linguistic variables such as negative big (NB), negative medium (NM), negative small (NS), zero (ZE), positive small (PS), positive medium (PM), and positive big (PB) being basic fuzzy sets.

The membership functions of the input variables and output variables are as shown in Fig. 16. The rule base is given in Table 6.

Five triangular membership functions have been allocated for input and output variables. Mamdani's method of fuzzification and centroid method of defuzzification have been used for implementing the FL-based MPPT algorithm. The membership functions of input and output

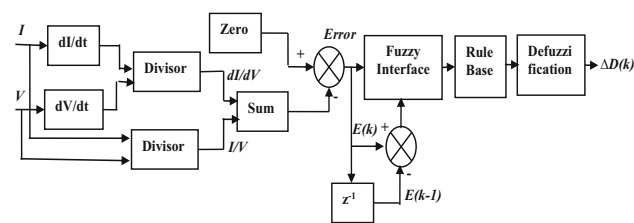


Fig. 13 Block diagram of FL-based MPP tracking

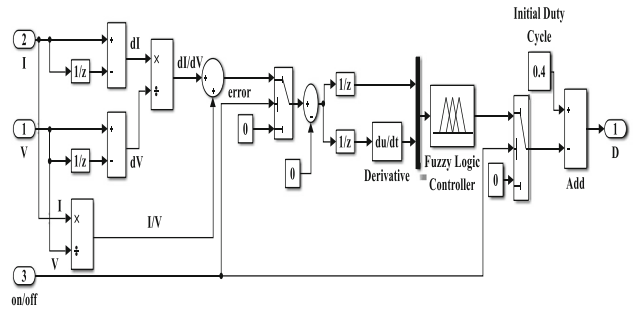


Fig. 14 Subsystem for FL-based MPPT controller

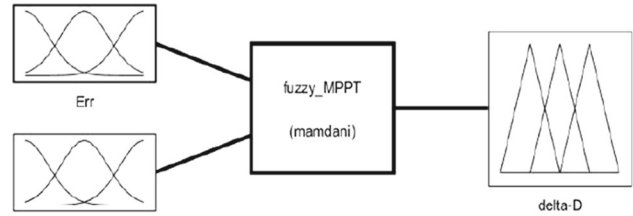


Fig. 15 FL-based MPPT algorithm with two inputs and one output

variables are shown in Fig. 17. The interval range of  $(-6, 6)$ ,  $(-250, 250)$  are used for input variables  $E(k)$  and  $\Delta E(k)$  and for output variable  $\Delta D$   $(-0.2, 0.2)$  for WT system. The rule base is given in Table 7. The linguistic variables such as negative big (NB), negative small (NS), zero (ZE), positive small (PS), and positive big (PB) being basic fuzzy sets.

Similarly, in the FC system, the triangular type membership functions of input and output variables are shown in Fig. 18. The range of membership functions are  $(10, 12)$ ,  $(46.5, 49)$  for input variables  $E(k)$  and  $\Delta E(k)$  and output variable  $\Delta D$   $(-0.2, 0.2)$  for FC system. The rule base is given in Table 8. The linguistic variables such as negative big (NB), negative small (NS), zero (ZE), positive small (PS), and positive big (PB) being basic fuzzy sets.

The model of FL-based MPPT controller is shown in Fig. 19. The subsystem of FL-based MPPT controller is shown in Fig. 14. Input gain blocks added with the input variables have been included in the MPPT controller block as shown in Fig. 19.

### 4.3 Model of ANN-based MPPT controller

Block diagram representation of ANN-based MPPT control method is shown in Fig. 20. The inputs can be voltage, current and/or environmental data like solar radiation, wind speed, and hydrogen fuel rate or combination of all/any of these. The output of the ANN, is the duty ratio used to operate the dc–dc converter at MPP.

The input data to train the network can be obtained from experimental measurements or model-based simulation

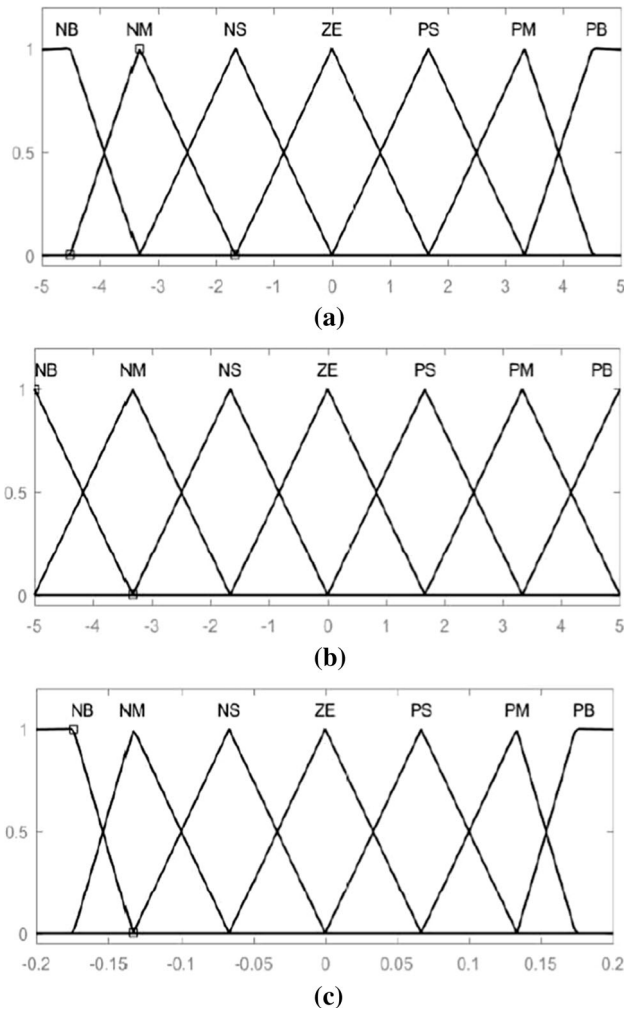


**Fig. 16** Input and output membership functions for PV system: **a** error ( $E$ ), **b** rate of change in error ( $\Delta E$ ) and **c** change in duty ratio ( $\Delta D$ )

results. The ANN can track the MPP after training it with the input data (Karanjkar et al. 2014b, c).

Neural network has been trained with an experimental set of input data using a Levenberg–Marquardt back propagation algorithm. A total of 1000, 5398, and 5000 samples were collected from the real-time experimental

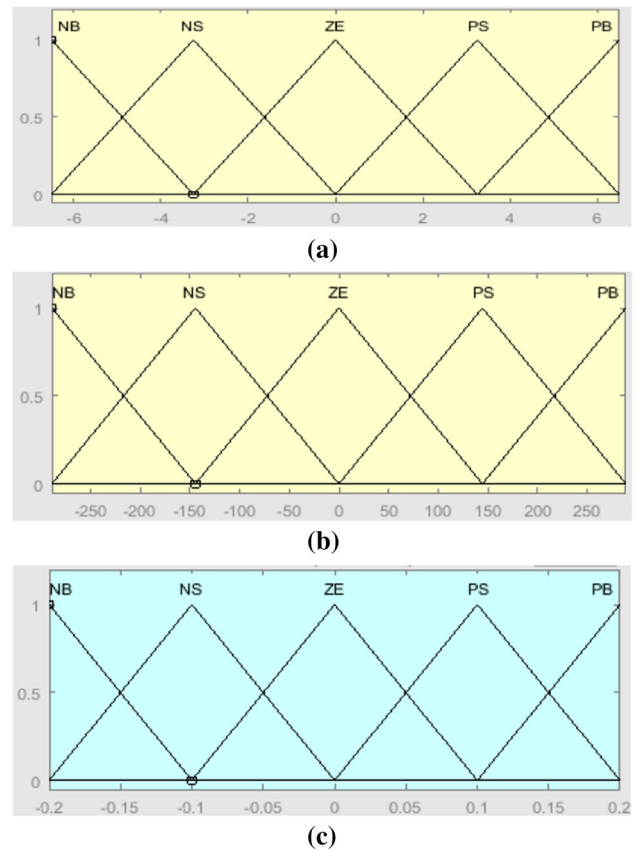


**Fig. 17** Input and output membership functions for WT system: **a** error ( $E$ ), **b** rate of change in error ( $\Delta E$ ) and **c** change in duty ratio ( $\Delta D$ )

setup of PV, WT and FC systems, respectively, out of which about 70% viz. 700, 3778 and 3500 samples were used to train the network while remaining samples were used for validation and testing purposes. These data samples (which are of voltage and current) are used to train an ANN for PV, WT, and FC model, respectively.

ANN-based MPPT controller has been modeled in MATLAB™/SIMULINK™ as shown in Figs. 21 and 22.

ANN-based MPPT controller is modeled as shown in Fig. 23, and ANN-based controller subsystem is shown in Fig. 21. Using this control method, to find maximum

**Table 6** Rule Base for FL MPPT Controller for PV System

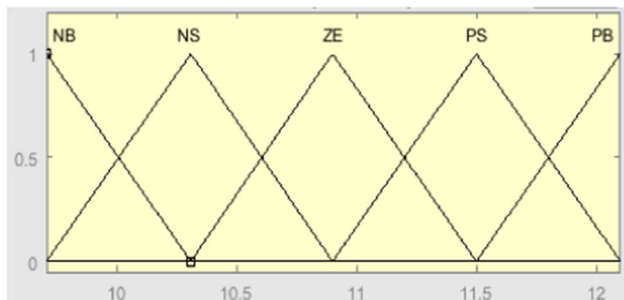
	Change in duty ratio (delta-D)	Error (Err)						
		NB	NM	NS	ZE	PS	PM	PB
Error rate (Err,ate)	NB	ZE	ZE	NM	NS	PB	PM	PB
	NM	ZE	ZE	NS	ZE	PB	PS	PB
	NS	ZE	ZE	ZE	ZE	PB	PS	PB
	ZE	NM	NB	ZE	NM	PB	PS	PB
	PS	NM	BB	ZE	NM	ZE	ZE	ZE
	PM	NM	NB	PS	NM	ZE	ZE	ZE
	PB	NM	NB	PM	NM	ZE	PS	ZE

**Table 7** Rule base for FL MPPT controller for WT system

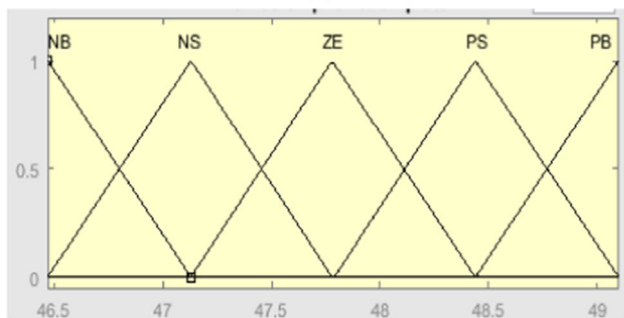
Change in Duty Ratio (delta-D)	Error (Err)	Error (Err)				
		NB	NS	ZE	PS	PB
Error Rate (Err,ate)	NB	NB	NS	NS	ZE	ZE
	NS	NB	NS	NS	ZE	PS
	ZE	NS	NS	ZE	PS	PS
	PS	NS	ZE	PS	PS	PB
	PB	ZE	ZE	PS	PS	PB

**Table 8** Rule Base for FL MPPT Controller for FC System

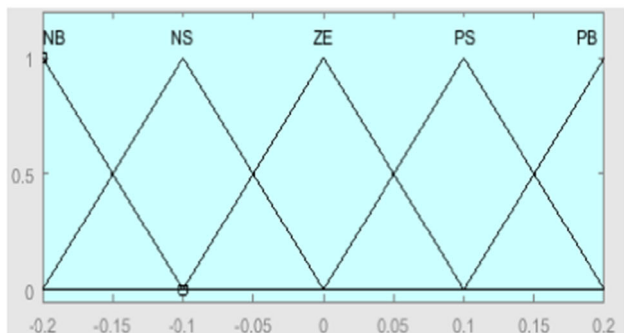
Change in duty ratio (delta-D)	Error (Err)	Error (Err)				
		NB	NS	ZE	PS	PB
Error rate (Err,ate)	NB	NB	NS	NS	ZE	ZE
	NS	NB	NS	NS	ZE	PS
	ZE	NS	NS	ZE	PS	PS
	PS	NS	ZE	PS	PS	PB
	PB	ZE	ZE	PS	PS	PB



(a)



(b)



(c)

**Fig. 18** Input and output membership functions for FC system: (a) error ( $E$ ), (b) rate of change in error ( $\Delta E$ ) and (c) change in duty ratio ( $\Delta D$ )

power from the system as compared to P&O and FL-based MPPT for PV, WT, FC, and HS.

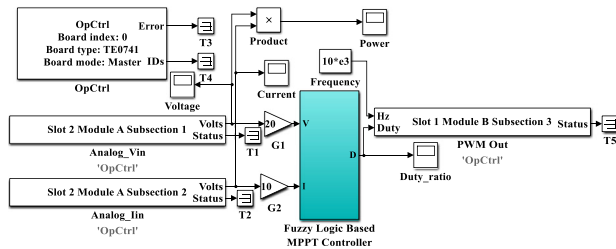


**Fig. 19** Model of FL-based MPPT controller in SIMULINK/OPAL-RT

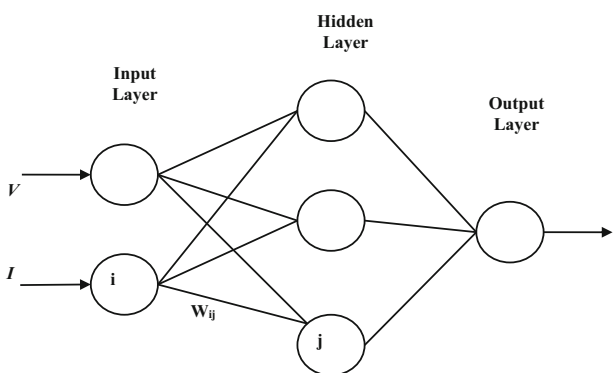


**Fig. 20** ANN-based MPPT technique

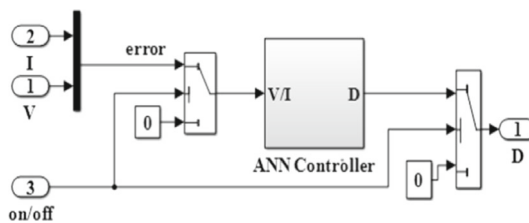


**Fig. 21** Subsystem for ANN-based MPPT controller

**4.4 Model of ANFIS-based MPPT controller**

In the present work, the ANFIS controller has been developed with two inputs: (1) voltage and ii) current and one output representing the duty ratio. In this controller, fuzzy rule base has to be generated based on Sugeno

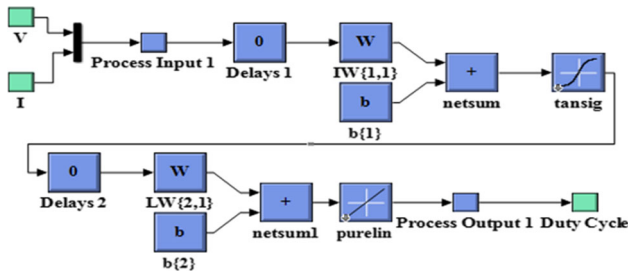


Fig. 22 Details of the subsystem of ANN controller

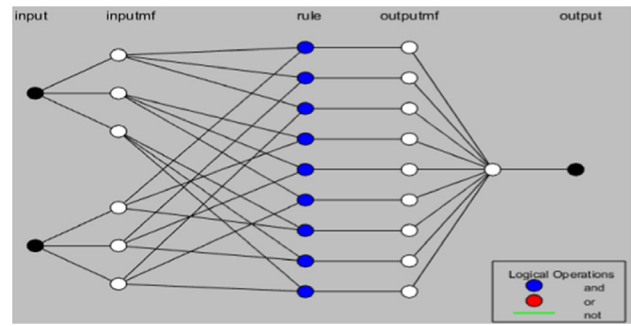


Fig. 25 ANFIS model structure

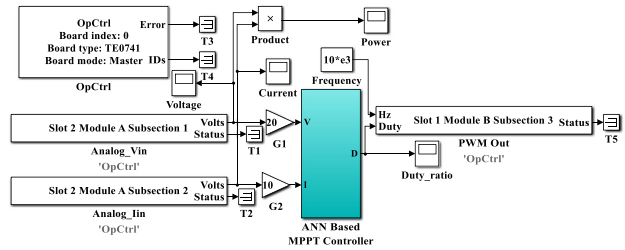


Fig. 23 Model of ANN-based MPPT controller in SIMULINK/OPAL-RT

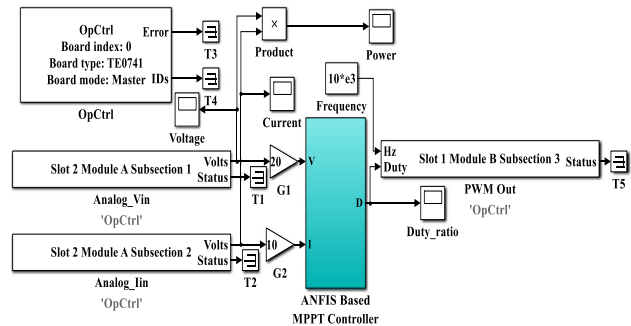


Fig. 26 Model of ANFIS-based MPPT controller in SIMULINK/OPAL-RT

inference model (Karanjkar et al. 2014b, 2014c). The ANFIS subsystem is shown in Fig. 24. Structure of the ANFIS model is depicted in Fig. 25.

The ANFIS-based MPPT controller has been developed in the present work, with two inputs and one output. This is shown in Fig. 26.

ANFIS-based controller has been designed with two neurons in layer 1 and 14 neurons in the fuzzification layer. Design procedure and training data are similar to that mentioned in the previous section. ANFIS-based MPPT controller provides the maximum power with no variations for PV, WT, FC, and HS as compared to other specified MPPT techniques.

### 5 Results and discussions

Results of the real-time simulator of different MPPT controllers applied to PV system with a boost converter, WT system with buck converter, FC with boost converter and HS have been illustrated in Figs. 27, 28, 29, 30, 31, 32, 33,

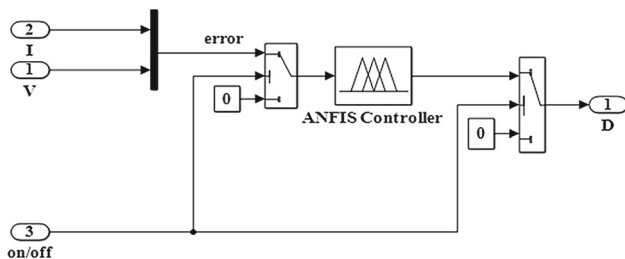


Fig. 24 Subsystem for ANFIS MPPT controller

34, 35, 36, 37, 38, 39, 40, 41, 42, 43, 44, 45. The response of input power and voltage of the boost converter for a PV system in real-time implementation is shown in Fig. 27. There is a large amount of fluctuations in this waveform. As the output of the system, depends on the radiation intensity, the waveforms have no specific characteristics, and may vary with change in radiation intensity. Figures 28, 29, 30, 31 shows fluctuations at start-up response time (or transient state) of boost converter because initially, the circuit components do not work properly. These fluctuations can be reduced by using optimized converters with hybrid MPPT techniques.

Real-time analysis using OPAL-RT simulator is performed in order to calculate MP from the PV array. The real-time simulation of the model has completed in 0.3 s as

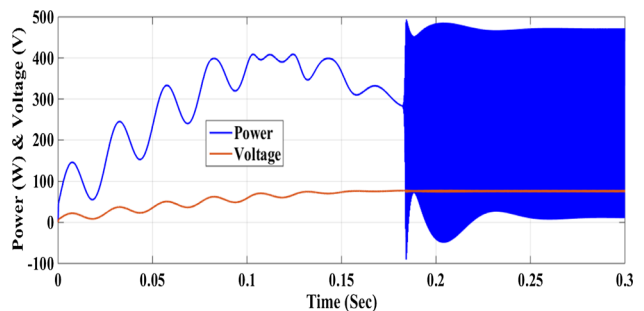


Fig. 27 Input response of boost converter for PV system

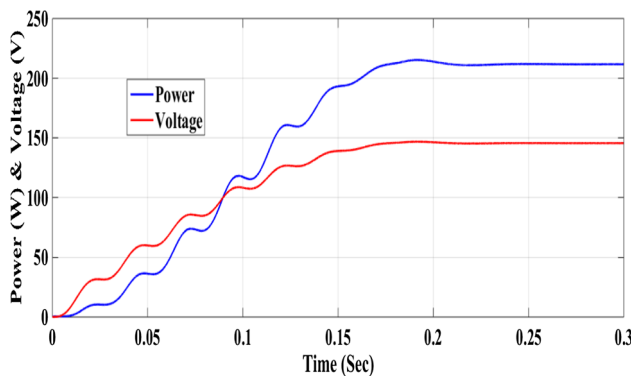


Fig. 28 Response of P&O MPPT controller incorporated with boost converter for PV system

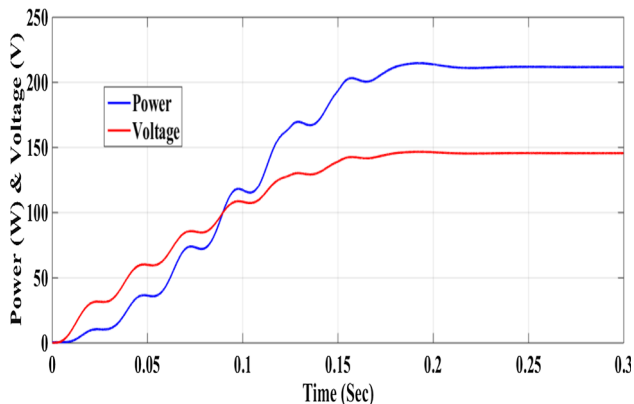


Fig. 29 Response of FL-based MPPT controller incorporated with boost converter for PV system

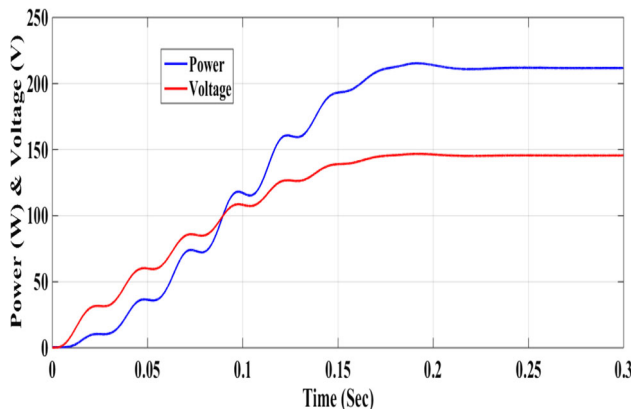


Fig. 30 Response of ANN-based MPPT controller incorporated with boost converter for PV system

the system attained steady-state condition within this period. In Fig. 29, it is clearly observed that the output power and voltage values of the boost converter with P&O MPPT controller are about 220 W and 145 V, respectively.

Figure 29 shows that the boost converter output in the form of power and voltage values with FL-based MPPT is about 225 W and 145 V, respectively, and Fig. 30 shows

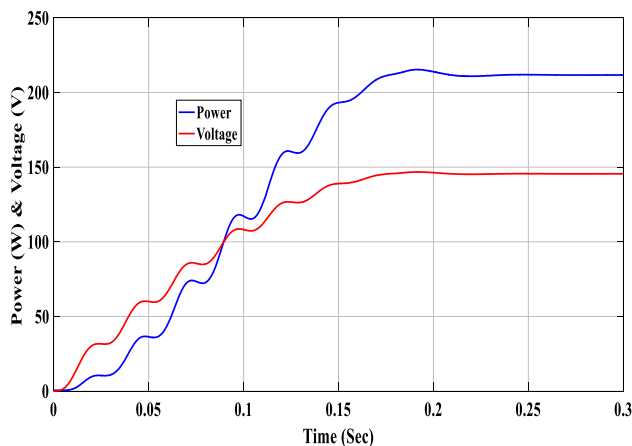


Fig. 31 Response of ANFIS-Based MPPT controller incorporated with boost converter for PV system

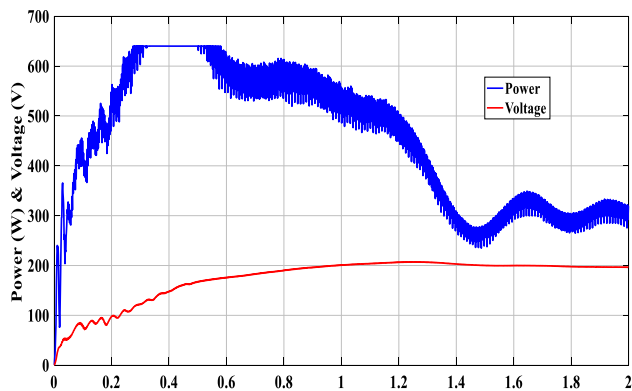


Fig. 32 Input response of buck converter for WT system

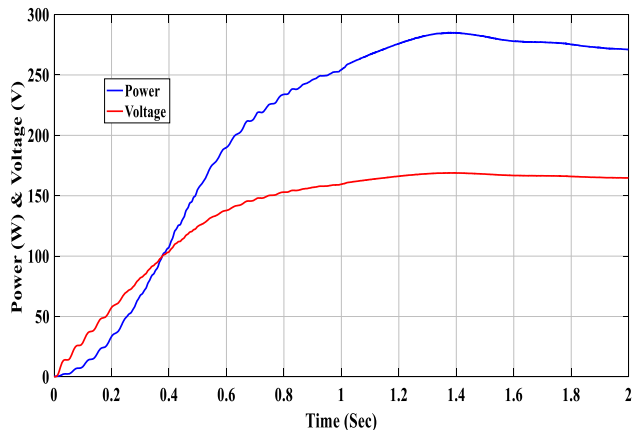


Fig. 33 Response of P&O MPPT controller incorporated with buck converter for WT system

that the output power and voltage values of a boost converter with ANN-based MPPT controller are about 230 W and 145 V, respectively. Figure 31 shows that the output power and voltage values of a boost converter with ANFIS-based MPPT controller are about 235 W and 145 V,

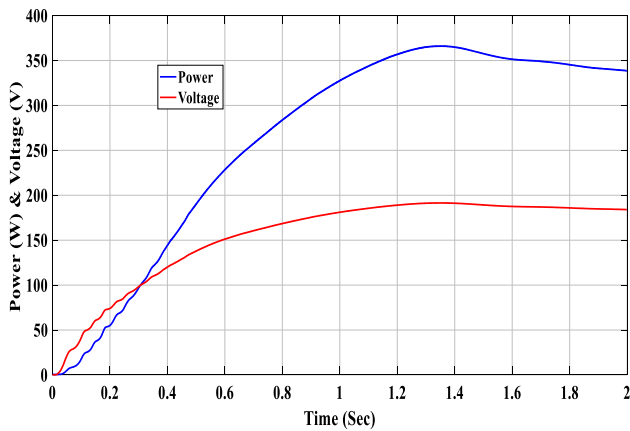


Fig. 34 Response of FL-based MPPT controller incorporated with buck converter for WT system

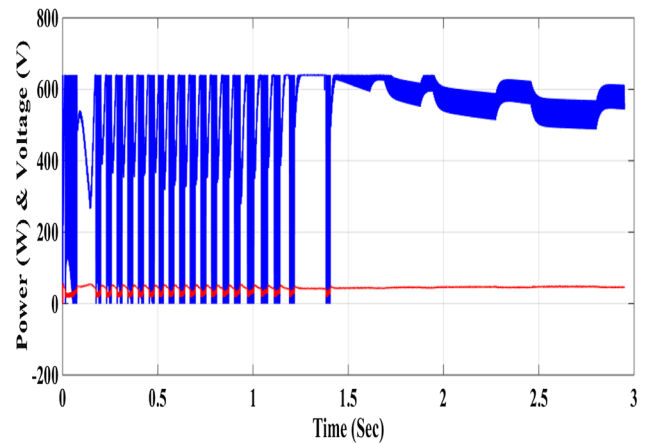


Fig. 37 Input response of boost converter for FC system

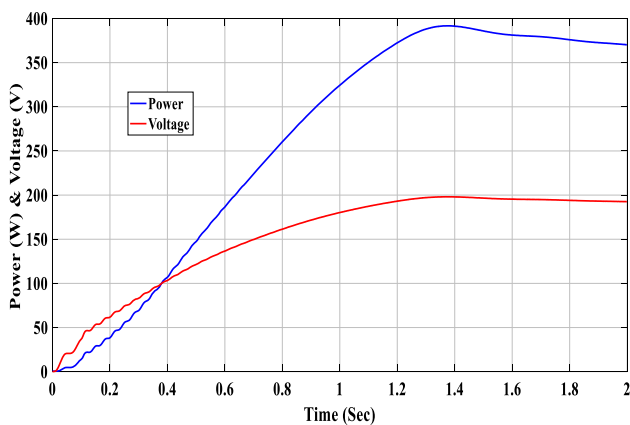


Fig. 35 Response of ANN-based MPPT controller Incorporated with Buck Converter for WT System

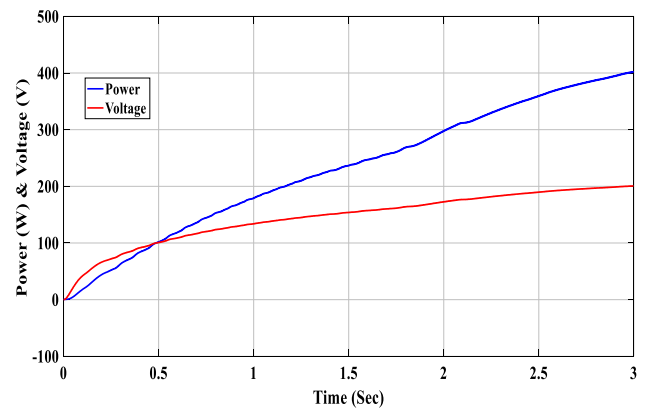


Fig. 38 Response of P&O MPPT controller incorporated with boost converter for FC system

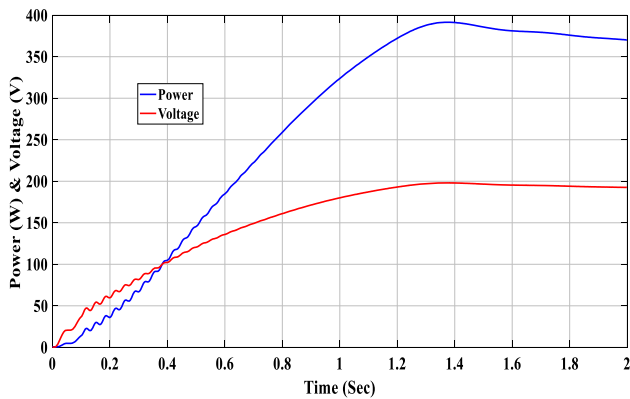


Fig. 36 Response of ANFIS-based MPPT controller incorporated with buck converter for WT system

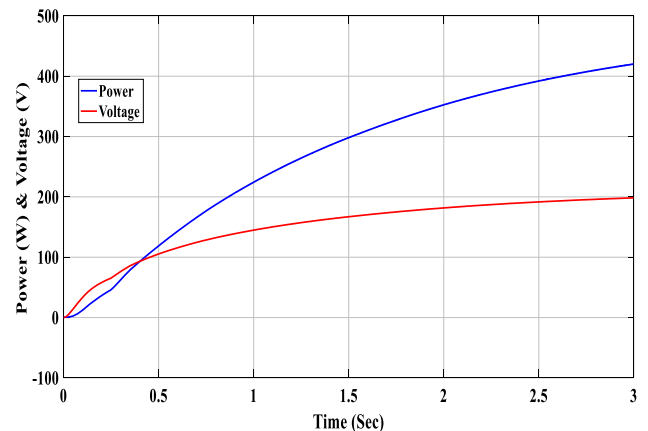


Fig. 39 Response of FL-based MPPT controller incorporated with boost converter for FC system

respectively. The ANFIS controller provides higher and accurate values of power and voltage as compared to P&O-, FL- and ANN-based MPPT controllers.

The input power and voltage of the buck converter for WT system are shown in Fig. 32. As the output of the

system, depends on the wind speed, the waveform has no specific characteristics, and it may vary with for other wind speeds.

In this case, the simulation has been carried out for 2 s. In Fig. 33, it is clearly observed that the output power and

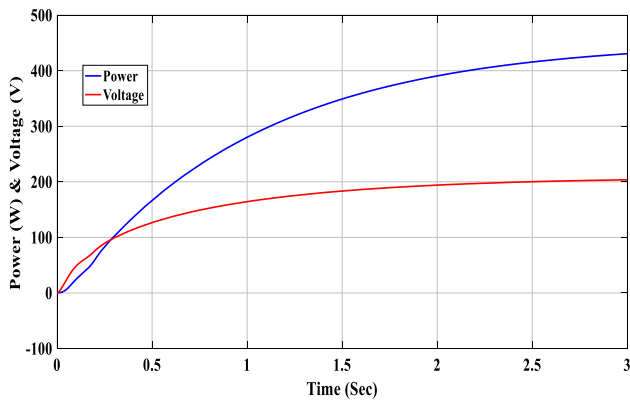


Fig. 40 Response of ANN-based MPPT controller incorporated with boost converter for FC system

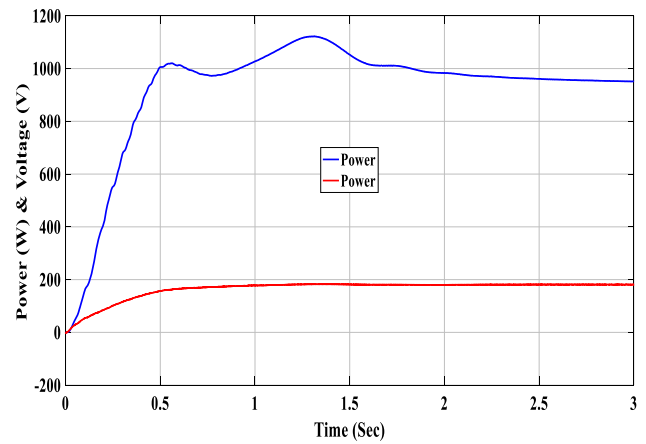


Fig. 43 Response of fuzzy logic-based MPPT controller for HS

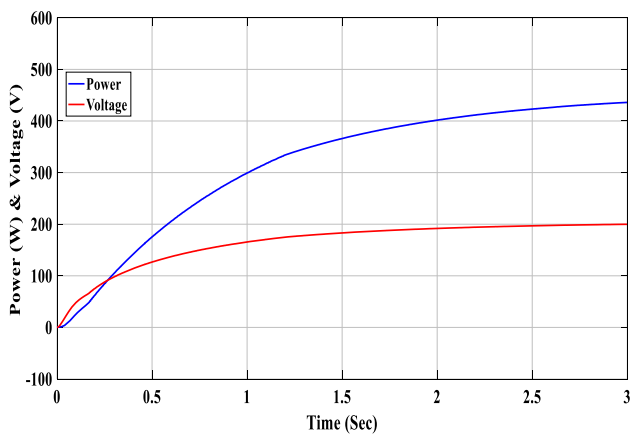


Fig. 41 Response of ANFIS-based MPPT controller incorporated with boost converter for FC system

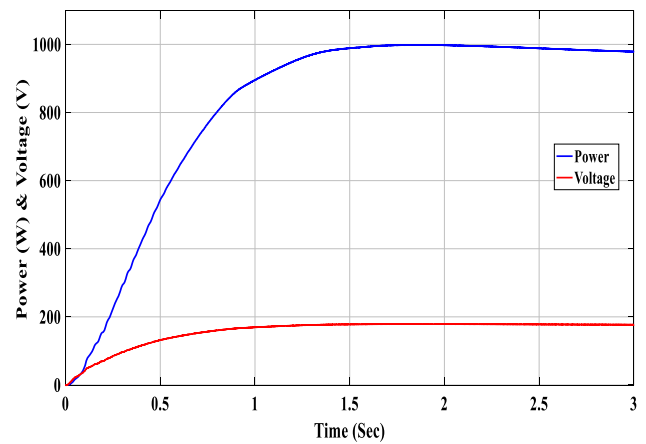


Fig. 44 Response of ANN-based MPPT controller for HS

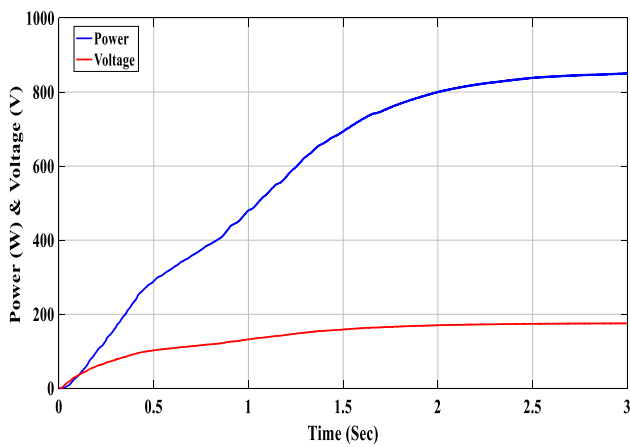


Fig. 42 Response of P&O-based MPPT controller for HS

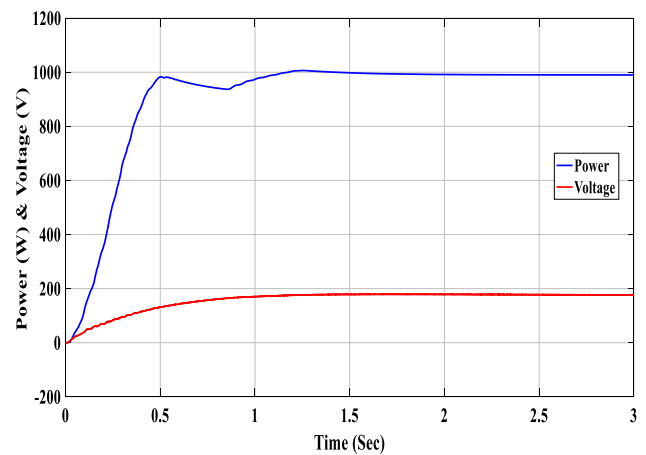


Fig. 45 Response of ANFIS-Based MPPT controller for HS

voltage values of the WT system with buck converter and P&O MPPT controller are about 290 W and 165 V, respectively.

Figure 34 shows that the output power and voltage values with FL-based MPPT are about 340 W and 180 V,

respectively, and Fig. 35 shows that the output power and voltage values with ANN-based MPPT controller are about 365 W and 180 V, respectively. The output power and voltage values with ANFIS-based MPPT controller as shown in Fig. 36 are about 375 W and 180 V, respectively.



Figure 37 shows the input response of power and voltage of the boost converter for FC system in real-time implementation. In this case, the output of the system, depends on the hydrogen fuel rate and circuit components, and hence the waveform has no specific characteristic. The simulation time considered is 3 s in this case, because the system attained steady state after that much time.

The responses of the different MPPT controllers on the FC systems after real-time implementation using OPAL-RT simulator are shown in Figs. 38, 39, 40, 41. In Fig. 38, the output power and voltage values of the FC system with boost converter with P&O MPPT controller are about 400 W and 200 V, respectively. From Fig. 39, the boost converter output power and voltage values with FL-based MPPT are about 420 W and 200 V, respectively. The output power and voltage values with ANN-based MPPT controller are about 430 W and 200 V, respectively, and the output power and voltage values of ANFIS-based MPPT controller are about 435 W and 200 V, respectively.

Similar experimentation has been carried out on the HS, whose laboratory setup is shown in Fig. 5. The real-time simulation is carried out for 3 s and the different responses have been observed with different MPPT controllers. Figures 42, 43, 44, 45 show these responses.

Observing Figs. 42, 43, 44, 45 carefully to calculate the output power and output voltage values of the system, the following values are obtained. The output voltage value is found to be same as 175 V for all the systems. The output

power value of the HS with P&O MPPT controller is about 850 W, and with FL-based MPPT it is about 950 W and with ANN-based MPPT controller it is about 980 W. The output power with ANFIS-based MPPT controller is about 990 W.

Table 9 shows a comparative chart of output power and output voltage values of different systems when incorporated with different MPPT controllers. Table 10 shows the percentage power increase of HS as compared to individual PV, WT, FC systems in real-time implementation incorporated with different MPPT controllers.

## 6 Comparative analysis of various MPPT controllers for different systems in OPAL-RT

For comparison of the results of the real-time implementations of different systems with P&O-, FL-, ANN- and ANFIS-based MPPT controllers, the responses of output of PV system obtained have been combined together and drawn in one illustration as in Fig. 46.

Such combined illustrations are again drawn for WT, FC and HS as shown in Figs. 47, 48, 49, respectively. From Figs. 46, 47, 48, 49, it can be seen that the response of FL-based MPPT is faster than P&O MPPT controller. FL-based MPPT controller do not exhibit oscillations during

**Table 9** Real-time implementation based comparison of the different MPPT controllers with DC–DC converter

MPPT method	PV system		WT system		FC system		HS	
	Output power (W)	Output voltage (V)	Output power (W)	Output voltage (V)	Output power (W)	Output voltage (V)	Output power (W)	Output voltage (V)
P&O	220	145	290	165	430	200	850	175
FL	225	145	340	180	435	200	950	175
ANN	230	145	365	180	420	200	980	175
ANFIS	235	145	375	180	400	205	990	175

**Table 10** Comparison of increased percentage power of HS in real-time implementation

MPPT method	Percentage (%) power increase in HS as compared to individual PV, WT, and FC system while real-time implementation		
	PV	WT	FC
P&O	286	193	98
FL	322	179	118
ANN	326	168	133
ANFIS	321	164	148

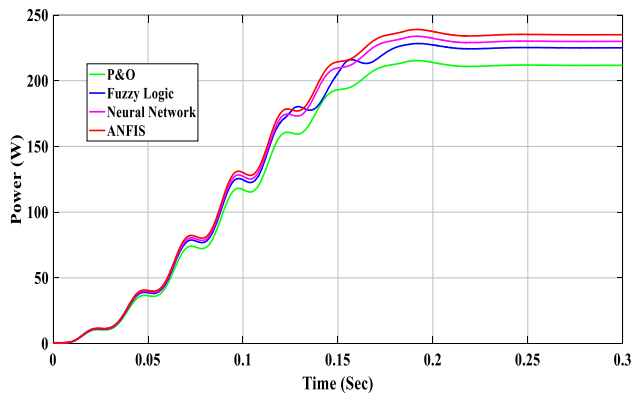


**Fig. 46** Response of output power for PV system with P&O, FL, ANN, and ANFIS to the variation in radiations

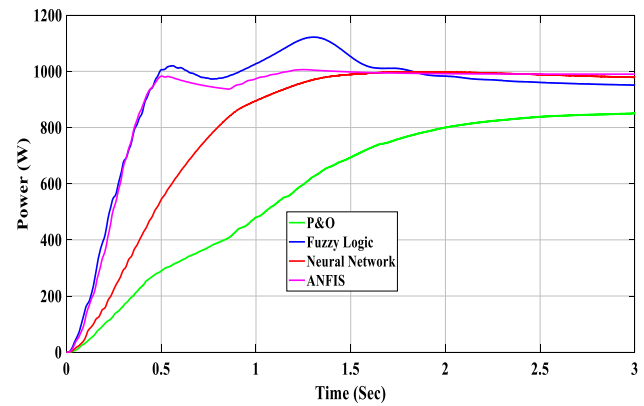


**Fig. 49** Response of hybrid model power with P&O, FL, ANN, and ANFIS to the variation in radiation, wind speed and hydrogen fuel rate

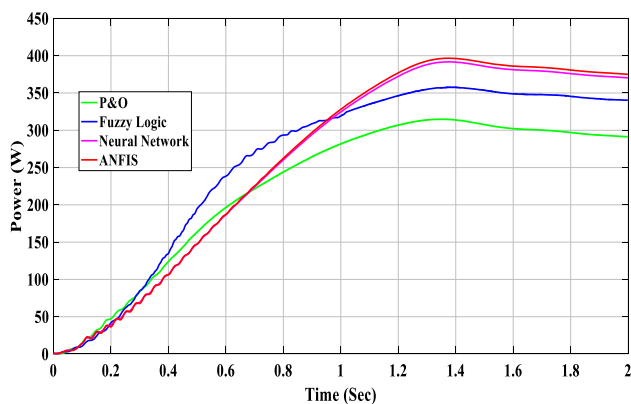


**Fig. 47** Response output power of WT system with P&O, FL, ANN, and ANFIS to the variation in wind speed

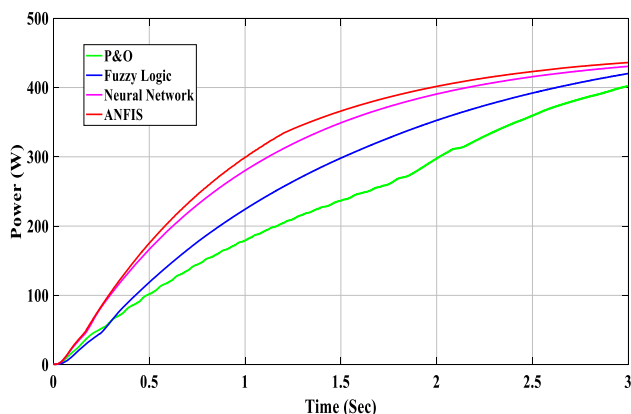


**Fig. 48** Response of FC power with P&O, FL, ANN, and ANFIS to the variation in hydrogen fuel rate

steady state while oscillation has been offered by P&O controller.

Artificial Intelligence (AI)-based controllers such as FL, ANN, and ANFIS-based MPPT controllers exhibits lesser

oscillations and better efficiency compared to all the four MPPT techniques. ANFIS-based MPPT controller offers maximum power. From the above arguments, it is clear that ANFIS-based MPPT controller gives best results.

## 7 Conclusions

Real-time implementation and comparative analysis of different MPPT controllers have been presented in this paper. MATLAB<sup>TM</sup>/SIMULINK<sup>TM</sup> models of different MPPT techniques have been developed and real-time simulations have been carried out on a prototype of solar PV system with a boost converter, WT system with buck converter, fuel cell system with boost converter and HS. OPAL-RT simulator has been used for interfacing voltage and current sensors and for generating PWM output signal. Performance comparison of MPPT techniques under a rapid change in radiation, wind speed has been presented based on tracking efficiency, steady-state and dynamic behaviors.

## Compliance with ethical standards

**Conflict of interest** Authors have no conflict of interest.

## References

- Algazar MM, Al-Monier H, El-Halim HA, Salem MEE (2012) Maximum power point tracking using fuzzy logic control. *Electrical Power Energy Syst* 39:21–28
- Ali AN (2014) An ANFIS based advanced MPPT control of a wind-solar hybrid power generation system. *Int Rev Modelling Simul* 7(4):638–643
- Entchev E, Yang L (2007) Application of adaptive neuro-fuzzy inference system techniques and artificial neural networks to

- predict solid oxide fuel cell performance in residential micro-generation installation. *J Power Sources* 170(1):122–129
- Giraud F, Salameh ZM (2001) Steady-state performance of a grid-connected rooftop hybrid wind-photovoltaic power system with battery storage. *IEEE Trans Energy Convers* 16(1):1–7
- Hasikos J, Sarimveis H, Zervas PL, Markatos NC (2009) Operational optimization and real-time control of fuel-cell systems. *J Power Sources* 193(1):258–268
- Kamal E, Koutb M, Sobaih AA, Abozalam B (2010) An intelligent maximum power extraction algorithm for hybrid wind–diesel-storage system. *Int J Electr Power Energy Syst* 32(3):170–177
- Karanjkar DS, Chatterji S, Kumar A, Shimi SL (2014) Fuzzy adaptive proportional-integral-derivative controller with dynamic set-point adjustment for maximum power point tracking in solar photovoltaic system. *Syst Sci Control Eng An Open Access J* 2(1):562–582
- Karanjkar DS, Chatterji S, Shimi SL, Kumar, A. (2014, March). Real time simulation and analysis of maximum power point tracking (MPPT) techniques for solar photo-voltaic system. In IEEE conference on Recent Advances in Engineering and Computational Sciences (RAECS), pp. 1–6
- Karanjkar DS, Chatterji S, Shimi SL, Kumar A (2014) Real time simulation and analysis of maximum power point tracking (MPPT) techniques for solar photo-voltaic system. In IEEE, Recent Advances Engineering and Computational Sciences (RAECS), Chandigarh, India (pp. 1–6)
- Kewat S, Singh B, Hussain I (2018) Power management in PV-battery-hydro based standalone microgrid. *IET Renew Power Gener* 12(4):391–398
- Khan MJ (2020) Review of recent trends in optimization techniques for hybrid renewable energy system. *Arch Comput Methods Eng*. <https://doi.org/10.1007/s11831-020-09424-2>
- Khan MJ, Mathew L (2018) Comparative analysis of maximum power point tracking controller for wind energy system. *Int J Electron* 105(9):1535–1550
- Khan MJ, Yadav AK, Mathew L (2017) Techno economic feasibility analysis of different combinations of PV-Wind-Diesel-Battery hybrid system for telecommunication applications in different cities of Punjab, India. *Renew Sust Energy Rev* 76:577–607
- Leedy AW, Guo L, Aganah KA (2012) A constant voltage MPPT method for a solar powered boost converter with DC motor load. In Proceedings of IEEE Conference on South east con, (pp. 1–6)
- Masoum MA, Dehbonei H, Fuchs EF (2002) Theoretical and experimental analyses of photovoltaic systems with voltage and current-based maximum power-point tracking. *IEEE Trans Energy Convers* 17(4):514–522
- Meiqin M, Jianhui S, Chang L, Guorong Z, Yuzhu Z (2008) Controller for 1kW–5kW wind-solar hybrid generation systems. In IEEE Canadian Conference on Electrical and Computer Engineering (CCECE), (pp. 001175–001178)
- Mousavi SM, Fathi SH, Riahy GH (2009) Energy management of wind/PV and battery hybrid system with consideration of memory effect in battery. In IEEE Conference on Clean Electrical Power, (pp. 630–633)
- Pak L, Faruque MO, Nie X, Dinavahi V (2006) A versatile cluster-based real-time digital simulator for power engineering research. *IEEE Trans Power Syst* 21(2):455–465
- Rowe A, Li X (2001) Mathematical modeling of proton exchange membrane fuel cells. *J Power Sources* 102(1):82–96
- Shankar K, Thangaraj M, Abudhahir A (2013). Performance analysis of MPPT algorithms for enhancing the efficiency of SPV power generation system: a simulation study. In IEEE Conference on Emerging Trends in VLSI, Embedded System, Nano Electronics and Telecommunication System (ICEVENT), (pp. 1–5)
- Sharma MK, Soni SU (2016) Performance analysis of a standalone PV-Wind-diesel hybrid system using ANFIS based controller. *Int J Comput Appl* 147(13):18–23
- Tudorache T, Kisk D, Rădulescu B, Popescu M (2012) Design and implementation of an autonomous Wind/PV/Diesel/Battery power system. In IEEE Conference on Optimization of Electrical and Electronic Equipment (OPTIM), (pp. 987–992)
- Valenciaga F, Puleston PF (2005) Supervisor control for a stand-alone hybrid generation system using wind and photovoltaic energy. *IEEE Trans Energy Convers* 20(2):398–405
- Yadav AK, Malik H, Arif MSB (2018) Techno economic feasibility analysis of different combination of PV–wind–diesel–battery hybrid system. In Hybrid-Renewable Energy Systems in Micro-grids (pp. 203–218)

**Publisher's Note** Springer Nature remains neutral with regard to jurisdictional claims in published maps and institutional affiliations.